Multiscale Layered Biomechanical Model of the Pacinian Corpuscle

Abhijit Biswas, M. Manivannan, and Mandayam A. Srinivasan

Abstract—This paper describes a multiscale analytical model of the lamellar structure and the biomechanical response of the Pacinian Corpuscle (PC). In order to analyze the contribution of the PC lamellar structure for detecting high-frequency vibrotactile (VT) stimuli covering 10 Hz to a few kHz, the model response is studied against trapezoidal and sinusoidal stimuli. The model identifies a few generalizable features of the lamellar structure which makes it scalable for different sizes of PC with different number of lamellae. The model describes the mechanical signal conditioning of the lamellar structure in terms of a recursive transfer-function, termed as the Compression-Transmittance-Transfer-Function (CTTF). The analytical results show that with the increase of the PC layer index above 15, the PC inner core (IC) relaxes within 1 ms against step compression of the outermost layer. This model also considers the mass of each PC layer to investigate its effect on the biomechanical response of the lamellar structure. The interlamellar spacing and its biomechanical properties along with the model response are validated with experimental data in the literature. The proposed model can be used for simulating a network of PCs considering their diversity for analyzing the high-frequency VT sensitivity of the human skin.

Index Terms—Lamellar structure, viscoelastic property, biomechanical response, compression transmittance transfer function

1 Introduction

The Pacinian Corpuscle (PC) is the largest mechanoreceptor found in the human body. It is widely distributed in the skin, joints and viscera. After its discovery in 1741 by Lehmann [1], the anatomical description of its three major parts, the Nerve Fiber (NF), Inner Core (IC) or simply core, and perineural capsule were reported early in 1911 [2]. Although the last century witnessed its histochemical and anatomical detailing upto sub-micrometer level, only few studies have attempted to model its biomechanical properties mathematically [1], [3], [4]. These models, developed more than five decades ago, are not scalable considering the diversity in the PCs. To develop a scalable and more accurate model, we have summarized the anatomical details of its lamellar structure [1], [2], [5] including recent discoveries [1], [6], [7], [8], [9], [10] that are not considered in [3]. In addition, recent discoveries in histochemistry [1], [6], [8] lead to the identification of a few key features of the lamellar structure that can be used for developing a scalable model of the PC. A major application of such a model could be in the characterization of the Vibrotactile (VT) sensitivity of the skin and in understanding the physiology and pathology [11], [12] related to the PC.

The biomechanical response of the PC was first detailed in [4] and modeled in [3]. These two works indicate that the mechanism behind its extreme sensitivity toward high-frequency VT stimuli is the rapid biomechanical response of its IC and NF. The rapid adaptiveness of the PC core is found to be the result of mechanical signal filtering performed by the lamellar structure inside the capsule [4]. Based on these results, Loewenstein and Skalak [3] developed the first biomechanical model of the PC. Though the model response does not match the experimental results well [13], [14] and the mass of the layers was also neglected, the theoretical analysis in [3] offers a valuable framework to build a more accurate and generic model of the PC. Another drawback of the model in [3] is that it treats the IC and NF as rigid objects. This assumption is a serious limitation restricting the integration of biomechanical and neurophysiological models, as rigid objects cannot be stretched and the stretch-activated ion channels in the axolemma are critical for mechanotransduction [9], [15].

The main objective of this paper is to analyze the effect of size variability of the PC by developing a scalable layered biomechanical model which can describe the experimental relaxation response [4] more accurately than that of [3]. Therefore, first, we have proposed a generalized relationship between the PC size and the number of lamellae present in it. Though we have modeled the PC as concentric fluid-filled cylinders similar to [3], it includes a more reasonable interlamellar spacing with a viscoelastic core in it. Next, we have considered the mass of each layer to investigate its effect on the frequency response even beyond 1 kHz. Moreover, appropriate material properties are chosen for matching the experimental results [4].

2 Model Description

2.1 Structural and Material Properties of the Layers

Perineural capsule. The PC capsule (Fig. 1) may contain 20-70 squamous epithelial lamellae of <0.5 μm thickness and the interlamellar spaces are filled with viscous fluid containing scattered collagen fibrils [1], [6], [8], [10]. Typically, each layer is separated by lamella which partly isolates the interlamellar

- *A. Biswas and M. Manivannan are with the Touch Lab, Biomedical Research Group, Department of Applied Mechanics, IIT Madras, Chennai 600036, India. E-mail: abhi.tech.2006@gmail.com, mani@iitm.ac.in.*
- *M. A. Srinivasan is with the Touch Lab, Department of Mechanical Engineering and the Research Laboratory of Electronics, MIT, Cambridge, MA 02139, USA, and the Touch Lab, Department of Computer Science, University College London, WC1E 6BT, United Kingdom. E-mail: srini@mit.edu.*

Manuscript received 6 Apr. 2014; revised 7 Sept. 2014; accepted 10 Sept. 2014. Date of publication 10 Nov. 2014; date of current version 13 Mar. 2015. Recommended for acceptance by D. Pawluk.
For information on obtaining reprints of this article, please send e-mail to: reprints@ieee.org, and reference the Digital Object Identifier below.
Digital Object Identifier no. 10.1109/TOH.2014.2369416

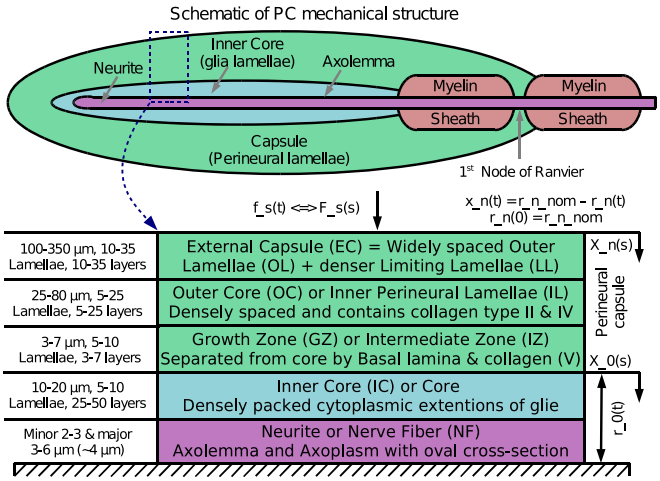

Fig. 1. Biomechanical model of the PC (lateral cross-section). The datum line represents the central axis of the neuron. The prefix '_' of the symbols in the figure indicates the subscripts as referred in the following section. *f_s(t)*: force on the outermost PC lamella, *F_s(s)*: Laplace transform of *f_s(t)*, *x_n(t)*: Compression over radius for the nth PC layer, *X_n(s)*: Laplace transform of *x_n(t)*, *r_n_nom*: nominal radius of the nth layer, *r_n(t)*: radius of the nth layer at time *t*.

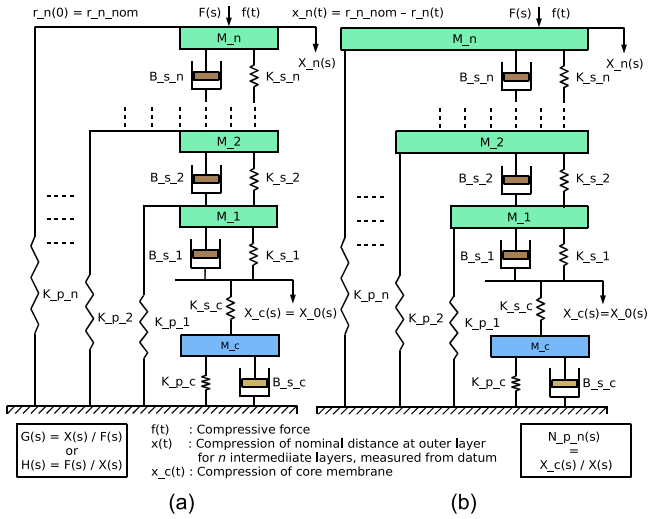

Fig. 2. Two possible biomechanical models of the PC based on relative arrangement of *K_p* and *M*. The prefix '_' of the symbols in the figure indicates subscripts as referred in the following section. *K_p*: Stiffness of parallel spring (representing lamella), *K_s*: Stiffness of serial spring (representing the elastic part of the interlamellar matrix), *B_s*: Viscous frictional coefficient of the serial damper (representing the fluidic part of interlamellar matrix), *M*: mass of each layer.

fluid from the next layer [16]. The perineural capsule is typically segmented into three zones [1], [10] (Fig. 1): the Growth Zone (GZ, the intermediate zone or innermost perineural lamellae), inner perineural lamellae (inner lamellae or Outer Core, or OC), and the external capsule (Outer Lamellae, or OL). Few outer Limiting Lamellae (LL) of the external capsule may also be considered as a separate zone [10]. These zones have different interlamellar spacing and compositions of extracellular matrix. However, these zones are not always distinctly identifiable under a microscope [10].

IC and neurite. The PC IC is constituted of closely spaced 25-50 layers of cytoplasmic extensions of specialized glia or Schwann cells. These cytoplasmic extensions are bilaterally wrapped around the oval axolemma [1], [2] of the neurite having the major and minor axis in the order of 6 and 12 μm [17]. The bodies of these glia are mainly found at the outer boundary of the IC. The IC (the outermost glia lamellae) is separated from the innermost perineural lamellae in the GZ by basal lamina and a narrow space (included in the GZ of Fig. 1) filled with an amorphous matrix of collagen fibrils and fine filaments [6], [10].

Heterogeneity of the capsule. The PC capsule has inherent heterogeneity both in interlamellar spacing and in the material properties of the interlamellar matrix. The innermost lamellae of the GZ consist of densely packed multilamellar complexes networked with a collagen matrix derived from fibroblasts [6]. After GZ, the lamellae are spaced more than a few μm in the OC and the spacing increases in the order of 10 μm at the periphery of the external capsule after the OC [8] (Fig. 1). However, the outermost 5-7 lamellae of the external capsule are closely spaced and densely packed with collagen fibrils [6]. Throughout all the layers of the perineural capsule, the lamellae are attached with the basal lamina and the extracellular matrix scattered with collagen fibrils.

2.2 Model Parameters and Approximations

The PC is approximated as concentric cylinders filled with viscous fluid in each layer, which is similar to [3] but with several major improvements. Each layer of the lamellar structure is modeled with four elements: two springs (parallel K_p and serial K_s), damper (B_s), and a mass (M) (Fig. 2). As the PCs may have different numbers of lamellae (Fig. 1), the developed model is parameterized with n (number of layer). The following parameters are used in the developed model.

n: Number of lamellae present in the PC capsule
i: Layer index ($0 \le i \le n$) and core is the 0th layer
m: Layer index ($1 \le m \le n$)
R_i: Nominal radius (*r_i_nom* in Fig. 1) of the ith layer
E_{Li}: Elastic modulus of the ith lamella
E_{Mi}: Elastic modulus for the ith interlamellar matrix
U_i: Viscosity of the fluidic part of the matrix
L: Length of the lamellae (1 mm for all layers)
T : Thickness of the ith lamella
S_i: Thickness of the ith interlamellar space
C_i: Cumulative thickness of the ith interlamellar space
A_i: Radial surface area of the ith layer
D_i: Density of the ith layer

Approximations considered in the developed model are listed in the following section.

a) The term "layer" includes a lamella and interlamellar matrix adjacent to it. However, occasionally more than one lamella jointly forms the layer separator in reality [16], which is treated as a single lamella for the purpose of modeling.
b) Interlayer material properties can be inhomogeneous but the intralayer material properties are homogeneous.
c) The interlamellar fluid is incompressible viscoelastic.
d) Although the fluid in the capsule can move among the adjacent interlamellar spaces with a significant amount of resistance [5], this model assumes no leakage among the layers (similar to [3]). In reality such isolation is mostly found in-between the IC and the perineural capsule for the purpose of electrical isolation [1].

e) All other approximations such as approximation of the shape of the PC as a concentric cylinder, equal length of all the layers and consideration of a linear biomechanical model for individual layers as in [3] are equally applicable in this model.

2.3 Analytical Relationship of Model Parameters

From Hubbard's experimental findings [4] it is possible to segment different zones of the capsule either in terms of radii (1) or layer indices (2). The different zones in the lamellar structure can be segregated in terms of the LL, OL, OC, and GZ (Fig. 1). Typically, LL and OL can be combined as the External Capsule (EC). However, Hubbard segmented the capsule into only two zones, the EC and the OC, considering the GZ as its integrated part. Following [1], [4] the radius of the i[th] lamella of the PC can be expressed as:

$$R_i = R_0\,\gamma^i;\ where\ \gamma = 1.1 \quad \forall\ R_i < 75\ \mu\text{m};\ else\ \gamma = 1.08. \tag{1}$$

For the PCs considered in [4], (1) can also be rewritten as (2) where $R_0 = \sim 30\ \mu$m.

$$R_i = R_0\,\gamma^i;\ where\ \gamma = 1.1 \quad \forall \quad i < 11\ else\ \gamma = 1.08. \tag{2}$$

Combining (1) and (2), it is appropriate to consider the first 10-15 OC lamellae cover till 75 μm of the PC radius. One of the limitations of (1) and (2) is that it does not consider the outermost 5-7 perineural lamellae which are closely spaced and densely packed with collagen fibrils [6]. Formulation of such relations (1) and (2) and generalizing over many variations of the PCs is always a challenging task. One of such challenges is to measure the radius of the PC lamella as it shrinks if punctured [2]. Therefore, the lamellar clearance estimated from the microscopic slides, as reported in [1], [7], [8], [9], [10], may not be the exact functional interlamellar spacing.

From the theoretical analysis of [3] the value of the parallel spring (*K_p_i* in Fig. 2) representing the PC Lamellae can be determined by (3),

$$K_{pi} = \frac{E_{Li}A_i}{\frac{R_i^2}{T_i}\left\{1+\frac{4L^2}{\pi^2 R_i^2}\right\}^2}; \quad \forall 0 < i \le n. \tag{3}$$

The series spring and the damper (*K_s_i* and *B_s_i* in Fig. 2) representing the viscoelastic fluid in-between the PC lamellae can be analytically expressed by (4) and (5),

$$K_{si} = \frac{E_{Mi}A_i}{R_i - R_{i-1} - T_i}; \quad \forall\ 0 < i \le n; \text{where } R_0 = \text{core-radius} \tag{4}$$

$$B_{si} = \frac{12U_iL^2A_i}{\pi^2(R_i - R_{i-1} - T_i)^3\left\{1+\frac{4L^2}{\pi^2R_i^2}\right\}}; \quad \forall\ 0 < i \le n. \tag{5}$$

2.4 Existing Model Limitations and Improvements

Although the PC is modeled as concentric fluid-filled cylinders similar to [3], the following list describes the major improvements in our model over the existing ones [3], [4].

a) The PC lamella thickness is found to be in the order of 0.09 to 0.4 μm [1], which is at least half the thickness of that considered in [3]. In our model the lamellae thickness increases following the Weibull Function (6).

$$T_i = T_{mn} + (T_{mx} - T_{mn})\left(1 - \exp\left(-\left(\frac{1}{\alpha}\right)^{\beta}\right)\right); \quad \forall\ 0 < i \le n$$
$$\text{where } \alpha = n \times 90\%, \beta = 2.5, T_{mn} = 0.1\ \mu\text{m and } T_{mx} = 0.4\ \mu\text{m}. \tag{6}$$

b) The PC core is modeled as a viscoelastic layer instead of a rigid object as in [3], because [9], [15], [18], [19] show that the neural activity of the PC is controlled by strain- or stretch-sensitive ion-channels due to the deformation of the core. The entire core along with the NF is considered as a single layer for the purpose of modeling as the PC core is densely packed with glia lamellae and collagen within a radius of a few 10s of μm (Fig. 1). We have assumed that a fraction of the overall core compression ($x_0(t)$) will represent the stretch signal applied on the stretch-sensitive axolemma of the PC.

c) The elastic modulus of the lamellae as described in [3] is modified considering recent discoveries related to the PC. Loewenstein and Skalak [3] assumed that the elastic modulus is the same as that of the blood vessels. They considered elastic modulus = 0.5 MPa which is in the range of the peak elastic modulus of blood vessels; moreover collagen fibers, one of the constituents of blood vessels, can offer even much higher elastic modulus (in the order of 100 MPa) [20], [21]. However, we have considered the elastic modulus in the order of 1 kPa due to the following reason. Histochemical and anatomical literature [2], [6], [10] show that all the PC lamellae in the perineural capsule are attached with basal lamina on both sides, which mainly consists of flexible type-IV basement-membrane-collagen and laminin [6], [8], [10], [22]. On the other hand, the walls of the blood vessels mainly have types I and III collagen and elastin matrix [23], [24], providing better structural strength. This indicates that the lamellae elastic modulus should be in the order of stiffness of individual cells, closer to 1 kPa [1], [25], [26], which is definitely much softer than the blood vessel wall. An attempt of directly measuring the elastic modulus of the PC has shown that its elastic modulus is in the order of 1 kPa [1], rather than 0.5 MPa.

d) In [3] the viscosity of the PC interlamellar fluid is considered to be the same as that of water which is also an over-approximation, as it has a significant concentration of collagen which can be more than 1,000 times viscous compared to water [27]. However, water being the major constituent of interlamellar fluid (~92 percent [1]), the viscosity of the fluid is assumed to be higher but comparable with that of the water (0.7 mPa.s at human body temperature). Therefore, a better choice of U_i would be 2-10 times than that of water.

e) The elastic component of the viscoelastic interlamellar matrix is the most influential parameter governing

the response of the PC, which is probably the most uncertain parameter in [3]. All the layers of the model in [3] have the same elastic modulus for the matrix which is 10^4 times less than that of the lamellae (E_{Li} : $E_{Mi} = 10^4$). Considering the recent literature [6], [10], it is clear that apart from the flexible type IV collagen, interlamellar spaces in the capsule are filled with a fluid containing scattered collagen fibrils of type II, and type V collagen is also found in the intermediate zone of perineural capsule [8]. Even the limiting interlamellar spaces of the capsule are densely packed with collagen [6]. Apart from collagen fibrils, elastic fibers are also found scattered in the interlamellar matrix [6]. As collagen may be 1,000 s of times stiffer [20], [21] than individual cell stiffness [1], [25], [26], the elasticity of the interlamellar matrix is governed by the type and density of collagen and elastic fibrils in it. Therefore, we have chosen E_{Mi} of (4) in the range of 1 Pa ($E_{Li} : E_{Mi} = 10^3$).

f) According to Hubbard's relation (1) and (2) the thickness of the ith interlamellar space (S_i) increases monotonically, which is found to be valid only for a small part of the PC capsule, whereas S_i is found to be reducing (non-monotonic) toward the LL of the capsule [1], [6], [10]. Probably for this reason Loewenstein and Skalak [3] could not simulate a PC with more than 30 layers, as the relation with 50 lamellae would result in an external diameter of 2.5 mm which is impractical. While measuring the radius of LL, Hubbard might have grouped a few of them together as they remain densely packed with collagen [6], [10]. Similarly the relationships (1) and (2) do not take care of the GZ of the capsule, as it indicates the $S_i > 1$ μm even in the GZ and OC, which contradicts the microscopic view of the PC cross-sections [1], [6], [9], [10], [16]. In order to generalize and improve the accuracy of the analytical relation between i and R_i we have followed a relativistic relationship considering n number of layers present in the capsule, where each zone contains a certain percentage of n lamellae (starting from the outermost layer of the PC, the first 10 percent layers are LL, the next 50 percent are the OL, the next 30 percent are the OC, and the next 10 percent are the GZ). Finding the exact value of n for a given PC is difficult compared to finding the R_n which itself is challenging as R_n shrinks if the capsule is punctured [2]. The relation among R_i, S_i, T_i and C_i are summarized in (7), where the parameter γ remains close to 1.3. The $\hat{R}_n$ (approximate value of R_n) can be measured under a microscope which could be 150–450 μm [1], [4], [5]. On the other hand R_0 (typically 10–20 μm) can be directly measured from the sectional view of the PC, as it has definitive boundary [1] which is less altered against external forces and preparation of microscopic slides,

$$S_i = (R_i - R_{i-1}) - T_i; \quad \forall\ 0 < i \leq n,$$
$$R_i = R_0 + (\gamma \hat{R}_n - R_0)\left(1 - \exp\left(-\left(\frac{1}{\alpha}\right)^{\beta}\right)\right) + i\,\delta; \tag{7}$$
$$\text{where, } \alpha = n \times 90\%, \beta = 2.5, \gamma = 1.3 \text{ and } \delta = 0.5\ \mu\text{m}.$$

g) In the literature the mass of the lamellar structure is neglected. The mass of each PC layer in this model is included in order to investigate its effect in transmission of mechanical stimulus. For estimating the mass of each layer, we have chosen the density of all layers close to water (1,000-1,100 kg/m^3).

2.5 CTTF from the PC Outer Layers to the Core

For modeling the mechanical signal transformation in the PC lamellar structure, we have introduced a dimensionless parameter Compression Transmittance Transfer Function (CTTF) $N_{pm}(s)$ relating the compression of the PC core (0th layer) as output, to the compression of the mth PC layer as input. The CTTF $N_{pm}(s)$ (for $m = n$) acts as a specialized high-pass filter for the mechanical compression at the outermost layer ($x_n(t)$ in Fig. 2).

Based on the relative arrangement of the parallel spring (K_{pi}) and mass (M_i) two equivalent models of the PC lamellar structure can be constructed (Fig. 2a and 2b). If mass is neglected and the core is considered as rigid, both of these models will be reduced to the model described in [3]. In our earlier model [28] we had considered the core layer ($i = 0$) as Kelvin's viscoelastic model with mass which yields a strictly-proper third order complex compliance (8). In this paper we preferred to model the core (Fig. 2) by Voigt's model (K_{pc}, B_{sc}) with mass (M_c) and a serial spring (K_{sc}), as it represents a bi-proper second order complex-compliance (9) which is more appropriate to model viscoelastic solids like soft tissues [29]. It is worth noting that another version of Kelvin's standard viscoelastic model with mass can also represent a bi-proper second order complex-compliance, which is not described in this paper [30],

$$G_0(s) = \frac{1}{H_0(s)} = \frac{X_0(s)}{F_0(s)} = \frac{1}{M_c s^2 + K_{pc} + \frac{1}{\frac{1}{B_{sc}s} + \frac{1}{K_{sc}}}}. \tag{8}$$

$$G_0(s) = \frac{1}{H_0(s)} = \frac{X_0(s)}{F_0(s)} = \frac{1}{M_c s^2 + B_{sc} s + K_{pc}} + \frac{1}{K_{sc}}. \tag{9}$$

Using the term $H_0(s)$ of (9), the $H_1(s)$ for the models (Figs. 2a and 2b) are given in (10) and (11) respectively,

$$H_1(s) = \frac{1}{G_1(s)} = K_{p1} + \frac{1}{\frac{1}{M_1 s^2 + B_{s1} s + K_{s1}} + \frac{1}{H_0(s)}}. \tag{10}$$

$$H_1(s) = \frac{1}{G_1(s)} = M_1\, s^2 + K_{p1} + \frac{1}{\frac{1}{B_{s1} s + K_{s1}} + \frac{1}{H_0(s)}}. \tag{11}$$

For ease of computation, we have considered the model shown in Fig. 2a and (10) for further analysis and recursively derived the CTTF $N_{pm}(s)$, relating the compression of the nth layer ($x_n(t)$) to the compression of the core layer ($x_0(t)$). In order to analyze the response of mechanical high-pass filter at intermediate layers of an n-layer PC, $x_m(t)$ for $1 \leq m \leq n$ are also simulated and corresponding CTTFs between the mth and 0th layers are denoted as $N_{pm}(s)$ (14).

The set of generalized equations defining the complex compliance ($G_i(s)$) for each layer can be written as:

$$G_0(s) = \frac{1}{H_0(s)} = \frac{X_0(s)}{F_0(s)} = \frac{M_c s^2 + B_{sc}\, s + (K_{pc} + K_{sc})}{K_{sc}(M_c s^2 + B_{sc}\, s + K_{pc})}$$

and

$$G_i(s) = \frac{1}{K_{pi} + \frac{1}{G_{si}(s)+G_{i-1}(s)}}; \quad \forall\, i = [1, 2, \ldots, n]$$

where

$$G_{si}(s) = \frac{1}{M_i\, s^2 + B_{si}\, s + K_{si}}; \quad \forall\, i = [1, 2, \ldots, n]. \tag{12}$$

In-between two consecutive layers the force transmittance $Q_{pi}(s)$ and compression transmittance $C_{pi}(s)$) can be summarized by (13),

$$Q_{pi}(s) = \frac{F_{i-1}(s)}{F_i(s)} = \frac{1}{1 + K_{pi}(G_{si}(s) + G_{i-1}(s))};\ \text{and}$$
$$C_{pi}(s) = \frac{X_{i-1}}{X_i(s)} = \frac{G_{i-1}(s)}{G_{si}(s) + G_{i-1}(s)}; \quad \forall\, i = [1, 2, \ldots, n]. \tag{13}$$

Hence, CTTF relating the compression of the m$^{\text{th}}$ layer to the core (0$^{\text{th}}$) layer of the PC can be written as:

$$N_{pm}(s) = \frac{X_0(s)}{X_m(s)} = \frac{G_0(s)}{G_{m-1}(s) + G_{sm}(s)}; \quad for\ m = 1$$
$$= \left\{\prod_{i=1}^{m-1} Q_{pi}(s)\right\} \frac{G_0(s)}{G_{m-1}(s) + G_{sm}(s)}; \quad \forall\, 2 \le m \le n. \tag{14}$$

It is easy to observe in (13) and (14) that if we neglect the effect of K_{pi} (if $K_{pi} = 0$ then $Q_{pi}(s) = 1$) the model gets reduced to a stack of Voigt's viscoelastic models on top of the core.

The products of $Q_{pi}(s)$ in (14) contain many closely spaced poles and zeros near the origin of the s-plane, which generally cause instability in simulation due to the limited digital resolution in the computational tool. Therefore, to avoid the instability, the compression $(x_i(t))$ of different PC layers is simulated recursively using $C_{pi}(s)$ (13). Another approach followed to avoid this instability is the approximation of the product of $Q_{pi}(s)$ form 1 to $m-1$ in the expression of $N_{pm}(s)$ (14), which could be $Q_{p(m-1)}(s)$ itself, as each $Q_{pi}(s)$ remains within the pass-band of $Q_{p(i-1)}(s)$ as well as $Q_{pi}(s)$ offering higher roll-off than $Q_{p(i-1)}(s)$ (referred in supplementary material, which can be found on the Computer Society Digital Library at http://doi.ieeecomputersociety.org/10.1109/TOH.2014.2369416, available online). The major advantage of this approximation is the reduction of computation time as it can directly simulate $x_0(t)$ from $x_n(t)$ without simulating the mechanical signal $(x_i(t))$ at all the PC layers between n and 0. This approximation makes the time-complexity of the simulation mostly independent of n for integrating this biomechanical model with the neurophysiological model of the PC [30], [31].

3 Results

3.1 The PC Layer Index versus Radius

The number of lamella in a PC capsule can vary from $n = 20$ to 70 and the peak layer thickness $(\text{Max}(R_i - R_{i-1}) = \text{Max}(S_i + T_i) \sim \text{Max}(S_i))$ typically reaches 10–15 μm [4], [10]. Therefore, we have simulated six typical PCs with 20, 25, 30, 40, 50 and 60 lamellae and considered that all these PCs have the same peak interlamellar spacing $(\text{Max}(R_i - R_{i-1}) = 12\ \mu\text{m})$ and accordingly calculated the R_i from (7) for each sample PC (Fig. 3a).

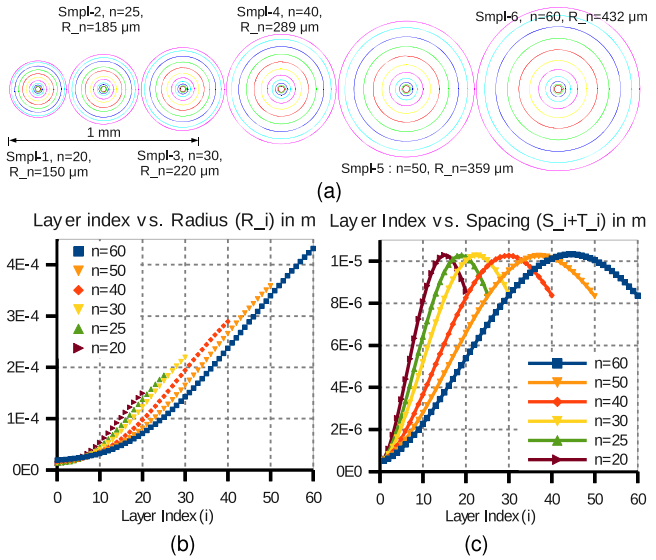

Fig. 3. (a) Axial cross-section of the six different sizes of the simulated PCs; Layers are sampled at every $i = 10\%$ of n for each PC starting from the IC ($i = 0$) till the outermost layer ($i = n$); (b) Layer index (i) versus radius of the i$^{\text{th}}$ layer (R_i); and (c) Layer index (i) versus interlamellar spacing ($(R_i - R_{i-1}) = (S_i + T_i)$) characteristics of six typical PCs considered for simulation ($n = 20$, 25, 30, 40, 50 and 60).

The analytical relations (6) and (7) are validated with the existing literature. The R_n and n obtained for the six simulated PCs are found to be highly reasonable (Fig. 3b) compared to that obtained from Hubbard's analytical relation (1) and (2) [1], [4], especially for a large value of n (>30). It is found that for the initial 4–10 layers (GZ), the interlamellar spacing S_i remains <1 μm which matches with [1], [6], [10], [16]. The lamellae thickness as calculated from (6), found to be restricted within 0.1 to 0.32 μm, also matches [1].

To quantify the model's accuracy, the analytical relation between i and R_i is compared with Hubbard's experimental result [4] which is the benchmark. However, it appears that due to insufficient magnification, Hubbard may have skipped indexing a few of the layers. The smallest possible interlamellar spacing reported by Hubbard is >1 μm [4]. This contradicts the modern high-magnification microscopic slides reported in [1], [6], [8], [9], [10], especially near the GZ. Therefore, Hubbard's experiment can be a benchmark with an index offset in the relation of i versus R_i and i versus $(S_i + T_i)$. The offset of six best matches the results from the proposed model, as well as the results from [3] (Fig. 4). As the experimental data from [4] explicitly indicate R_i for the 20 consecutive PC layers (with offset 6, i upto 26) for two typical PCs (Hb_Exp_1 and Hb_Exp_2 in Fig. 4), from the six simulated PCs we have selected $n = 25$ and 30 for comparing the results. Fig. 4 also includes the model results from Hubbard's analytical relation, denoted as Hb_Eqn. The R_i characteristic as reported in [3] is also included in Fig. 4 as Loe.

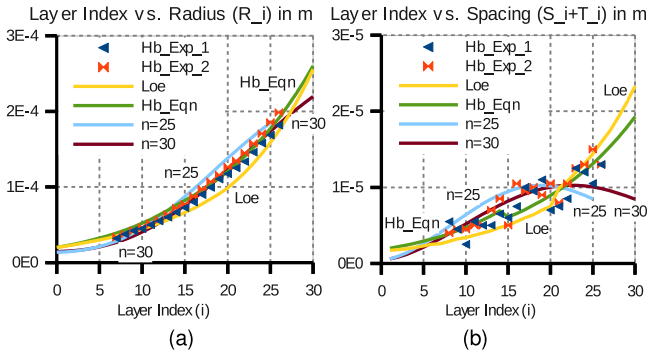

Fig. 4. (a) Layer index (i) versus radius of the ith layer (R_i); and (b) Layer index (i) versus interlamellar spacing ($(R_i - R_{i-1}) = (S_i + T_i)$) of the PCs with $n = 25$ and $n = 30$ layers, compared with experimental data in [4] (Hb_Exp_1 and Hb_Exp_2) and model in [3], [4] (Loe and Hb_Eqn).

The effect of an abrupt change of γ of the relation (1) and (2) is clearly observable as a step in Hb_Eqn (Fig. 4b between $i = 14$ and 15). A similar step is observable in Loe between $i = 20$ and 21. However, according to the microscopic slides, such a step is not very distinctive in general [1], [6], [8], [9], [10] and even for the slide in [4]. On the other hand the exponential rise of Hb_Eqn (Fig. 4) indicates that it is not suitable for modeling those PCs with a high number of layers ($n > 30$). Unlike Hb_Eqn, both the characteristics ($n = 25$ and $n = 30$ in Fig. 4b) from the proposed model indicate that the final few LL are closely spaced, which matches [6]. In comparison to [3], the proposed model better approximates Hubbard's experimental results for $n = 30$ in the range of $6 < i \leq 26$ (Table 1).

3.2 Zonal Segregation of the Lamellar Structure

Table 2 indicates the zonal segregation of the perineural lamellae (Fig. 1) based on the percentage of the total number of lamellae (n). In general the end of the GZ is considered at 10 percent of n. Similarly the end of the OC, OL and LL are considered at 40, 90 and 100 percent of n respectively.

The third column of Table 2 lists the number of lamellae present in each zone of the lamellar structure for the six simulated PCs (Fig. 3a). Apart from the number of layers in the different zones, columns 5-7 of Table 2 list the variation of the end-radius and zone-width based on the total number of layers of the PC (n). As shown in column 5 of Table 2, R_n as computed from (7) remains 3-4 percent higher than $\hat{R}_n$ (approximate value of R_n estimated from microscopic slides). The last three columns show the time constants for 25, 50 and 75 percent relaxation with respect to the peak compression of the terminal layer of each zone against a 32 μm radial step indentation at the outermost layer of PC ($i = n$).

TABLE 1
Comparison of Model Accuracy

	Layer radius (R_i)		Interlamellar spacing ($S_i + T_i$)	
	$n = 30$	Loe [3]	$n = 30$	Loe [3]
% mismatch w.r.t. layer-wise average of Hb_Exp 1 & 2				
SD over i	6.94	7.08	22.26	22.25
mean over i	−4.28	−10.26	5.23	−14.39
Correlation Coefficient w.r.t. Hb_Exp 1 & 2				
Hb_Exp_1	0.9982	0.9932	0.7944	0.8326
Hb_Exp_2	0.9981	0.9942	0.8458	0.8761

TABLE 2
Different Zones of PC and Relaxation Time

n : $\hat{R}_n$	Layers in Zones		Zone Boundary: Layer Index (i)	Zone Boundary: R_i (μm)	Zone Boundary: % of R_n	ZW: % of R_n	CR time constant: $\tau_{25\%}$ (ms)	CR time constant: $\tau_{50\%}$ (ms)	CR time constant: $\tau_{75\%}$ (ms)
20	IC	1	0% n = 0	12.6	8.4	8.4	0.659	0.71	1.024
:	GZ	3	10% n = 3	16.1	10.8	2.3	0.669	0.776	3.138
144	OC	6	40% n = 9	45.4	30.3	19.6	>300	>300	>300
μm	OL	10	90% n = 19	141.	94.3	63.9	>300	>300	>300
	LL	1	100% n = 20	149.7	100	5.7	inf	inf	inf
25	IC	1	0% n = 0	13.5	7.3	7.3	0.666	0.735	1.068
:	GZ	3	10% n = 3	16.4	8.9	1.6	0.672	0.763	1.67
178	OC	8	40% n = 11	52.5	28.4	19.6	>300	>300	>300
μm	OL	12	90% n = 23	167.1	90.5	62.1	>300	>300	>300
	LL	2	100% n = 25	184.6	100	9.5	inf	inf	inf
30	IC	1	0% n = 0	14.3	6.5	6.5	0.675	0.758	1.123
:	GZ	4	10% n = 4	18.5	8.4	1.9	0.685	0.811	2.128
212	OC	9	40% n = 13	59.6	27.2	18.7	>300	>300	>300
μm	OL	15	90% n = 28	202.2	92.1	65.0	>300	>300	>300
	LL	2	100% n = 30	219.5	100	7.9	inf	inf	inf
40	IC	1	0% n = 0	16.0	5.5	5.5	0.693	0.81	1.256
:	GZ	5	10% n = 5	21.0	7.3	1.7	0.705	0.864	1.97
280	OC	12	40% n = 17	73.9	25.5	18.3	>300	>300	>300
μm	OL	20	90% n = 37	263.2	91.0	65.4	>300	>300	>300
	LL	3	100% n = 40	289.3	100	9.0	inf	inf	inf
50	IC	1	0% n = 0	17.7	4.9	4.9	0.714	0.869	1.415
:	GZ	6	10% n = 6	23.5	6.5	1.6	0.727	0.929	2.003
348	OC	15	40% n = 21	88.3	24.6	18	>300	>300	>300
μm	OL	25	90% n = 46	324.3	90.3	65.7	>300	>300	>300
	LL	5	100% n = 50	359.1	100	9.7	inf	inf	inf
60	IC	1	0% n = 0	19.5	4.5	4.5	0.74	0.94	1.59
:	GZ	7	10% n = 7	26.1	6.0	1.5	0.75	1	2.12
419	OC	22	40% n = 25	103.2	23.9	17.9	>300	>300	>300
μm	OL	30	90% n = 55	387.8	89.8	65.9	>300	>300	>300
	LL	5	100% n = 60	431.8	100	10.2	inf	inf	inf

$\hat{R}_n$ is the approximate value of R_n used in (7); IC: Inner Core, GZ: Growth Zone; OC: Outer Core; OL: Outer Lamellae; LL: Limiting Lamellae; ZW: Zone Width; CR: Compression Relaxation; $\tau_{25\%}$, $\tau_{50\%}$ and $\tau_{75\%}$ are the time constants for 25, 50, 75 percent relaxation w.r.t. the peak compression of the individual layer, against 32 μm radial step indentation at the outermost layer of PC ($i = n$).

3.3 Layerwise Biomechanical Properties

The layerwise variation of the PC biomechanical properties is captured in three levels: (1) Elements (K_{pi}, K_{si}, B_{si} and M_i); (2) Complex compliance ($G_i(s)$); and (3) CTTF ($N_{pm}(s)$). In the following section the layerwise variations of these three parameters are discussed for $n = 30$, unless otherwise stated.

Variation of elements K_{pi}, K_{si}, B_{si} and M_i. The biomechanical properties K_{pi}, K_{si} and B_{si} (Fig. 2) as estimated using the relations (3), (4) and (5) are shown in Fig. 5. The simulation considers identical material properties for all layers ($E_{li} = 1$ kPa, $E_{mi} = 1$ Pa, $U_i = 3$ mPa.s, $D_i = 1{,}000$ kg.m^{-3} and $L = 1$ mm) in order to investigate the dependency of model response over i for the six simulated PCs (Fig. 3a).

Validation of K_{pi}, K_{si}, B_{si} and M_i. The existing model [3] describes only a 30-layer PC based on [4] and, therefore, in order to validate our model, the biomechanical properties of the PC layers in [3] are also included in Fig. 5, denoted as Loe. The stiffness of the lamellae and interlamellar matrix from the proposed model was found to be significantly

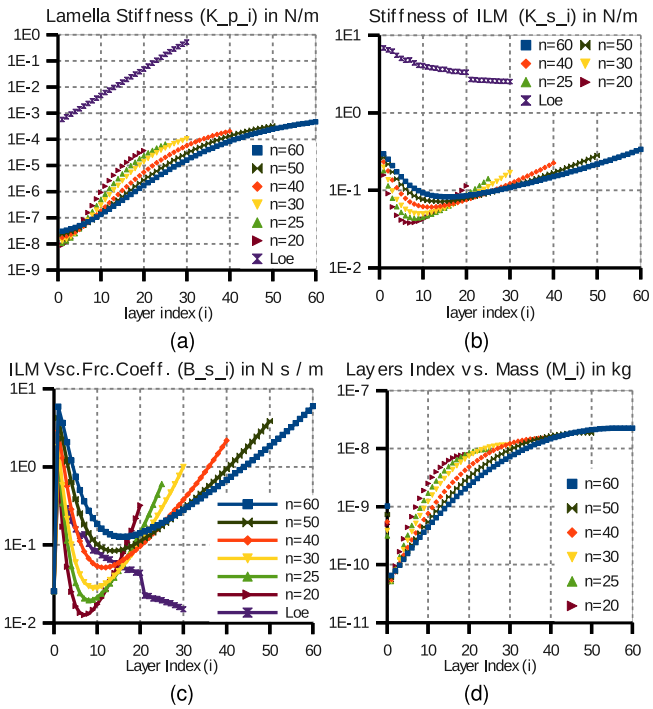

Fig. 5. (a): Stiffness of lamella (parallel spring *K_p* in Fig. 2a); (b): Stiffness of interlamellar matrix (serial spring *K_s* in Fig. 2a); (c): Viscous frictional coefficient of interlamellar matrix (damper *B_s* in Fig. 2a); and (d): Mass (*M* in Fig. 2a) of each layer for the PCs considered for simulation ($n = 20$, 25, 30, 40, 50 and 60) and in [3].

lower than that of [3] (Loe in Fig. 5), which is mostly due to lower E_{li} and E_{mi}, as mentioned in Section 2.4. Similarly the nonmonotonicity of the characteristic $n = 30$ (for K_{pi}, K_{si} and B_{si}) compared to Loe in Fig. 5 is mainly due to the nonlinearity and nonmonotonicity in the interlamellar spacing ($(R_i - R_{i-1}) = (S_i + T_i)$) of the PC (Fig. 3c).

Variation of complex compliance ($G_i(s)$) in terms of frequency and periodic step response. The frequency response of lamellar compliance ($G_i(s)$) of a 30-layer PC is given in Fig. 6(a). It also depicts the variation of $G_i(s)$ for $i = 1$, 4, 10, 16, 22, 28 and 30 (two terminal and five equally spaced internal layers) which belong to different zones of the PC layers (Table 2). The drop in the magnitude of $G_i(s)$ at higher frequencies indicates that the PC becomes stiffer as the frequency increases till a few kHz. On the other hand the phase difference between the compression and compressive force remains between -90 and -45 degrees in the range of 10-1,000 Hz for $i > 15$. The periodic step response (Fig. 6a bottom) indicates that the OL creep is higher than the inner lamellae due to larger interlamellar spacing and fluid content.

Variation of complex compliance ($G_i(s)$) in terms of a pole-zero map. As the poles and zeros of a transfer function govern the frequency response of a system, Fig. 6b shows the pole-zero map of minimal realization of the $G_i(s)$ with order reduction below 100 by performing stable pole-zero cancellation. The pole-zero map shows under-damped poles and zeros in Hz and sub-Hz range (Fig. 6b, top two panels). With increase of i not only does the number of poles and zeros increase in the PC lamellar structure but the pseudo-elliptical pole-zero map also increases its diameter. The relative placement of such a high number of

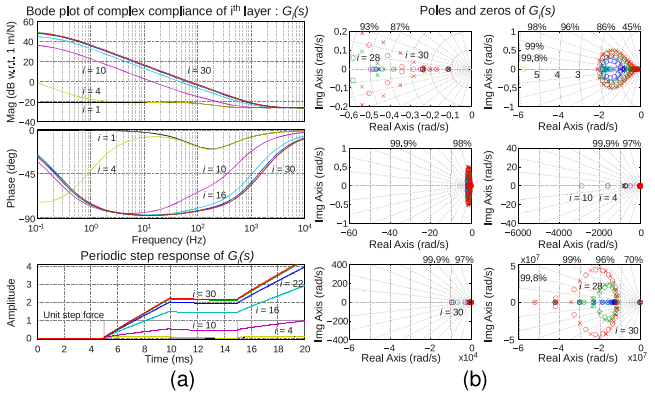

Fig. 6. Frequency response (Bode plot) (a top) and Periodic step response (a bottom) and pole-zero map; (b) of complex-compliance of the i[th] layer of a 30-layer PC ($G_i(s)$) for $i = 1$ (Black), 4 (Yellow), 10 (Magenta), 16 (Cyan), 22 (Blue), 28 (Green) and 30 (Red); The parameters with percentage indicate the damping factor corresponding to the radial grids. The pole-zero maps are zoomed out from top to bottom.

poles and zeros contributes to the curvature (slope change) of the frequency response characteristic (Fig. 6a top panel), which in combination governs its overall shape. On the other hand the larger diameter of the pole-zero map helps in preserving the effect of individual poles and zeros in the frequency response preventing the larger number of pole-zero cancellations effectively. Due to consideration of the mass of the PC layers, a second set of under-damped poles and zeros appears in the range of 1-10 MHz (Fig. 6b, bottom right panel). It is also clear that the damping factor of the under-damped poles and zeros can only be up to 90 percent, causing very little overshoot in the sub-Hz and MHz ranges. The low-frequency under-damped poles make soft tissue oscillate at Hz or sub-Hz frequencies against impact loading. However, the effect of MHz-range under-damped poles can be observed only against ultrasonic excitation as in [32]. Therefore, the effect of these second set of poles and zeros is negligible in the functional range of the PC.

Variation of CTTF ($N_{pm}(s)$) in terms of frequency and periodic step response. The high-pass filtering effect of the PC layers is clearly visible from the Bode plot and periodic step response of CTTF $N_{pm}(s)$ for $m = 1$, 4, 10, 16, 22, 28 and 30

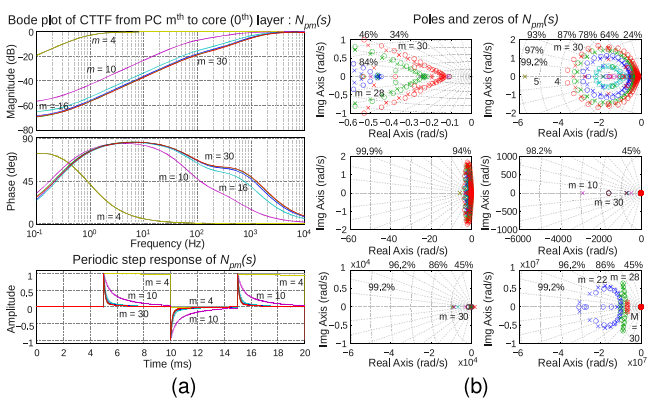

Fig. 7. Frequency response (Bode plot) (a top) and periodic step response (a bottom) and pole-zero map (b) of CTTF from the m[th] layer to the 0[th] layer (core) of a 30-layer PC ($N_{pm}(s)$) for $m = 1$ (Black), 4 (Yellow), 10 (Magenta), 16 (Cyan), 22 (Blue), 28 (Green) and 30 (Red); The parameters with percentage indicate the damping factor corresponding to radial grids. The pole-zero maps are zoomed out from top to bottom.

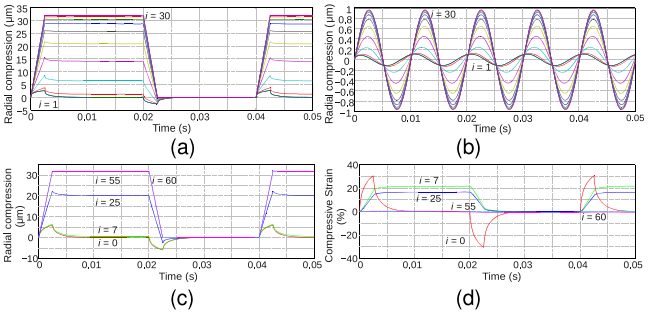

Fig. 8. Simulation of layer compression; An $n = 30$ layer PC stimulated with: (a) a periodic trapezoidal signal (freq = 25 Hz, radial amp = 32 μm and period to rise-time ratio = 16); (b) a sinusoidal signal (freq = 100 Hz, radial amp = 1 μm) where the layers are sampled at every 10 percent of n; (c) An $n = 60$ layer PC stimulated with a periodic trapezoidal signal with the same attributes as of Fig. 8a, where the layers are sampled at the zone boundaries (Table 2); and (d) percentile inter-layer strain corresponding to Fig. 8c.

(Fig. 7a). Considering the CTTF for the outermost layer ($n = 30$ and $N_{pm}(s) = N_{pn}(s)$), the slope of the magnitude spectrum changes significantly (~30 to ~10 dB/decade) within the functional range of the PC (a few 10s of Hz to a few kHz) and especially around 100 Hz. On the other hand the phase difference between the compressions of the nth layer to the 0th layer is found to be within 90 to 45 degrees. It is clear that with the increase of the number of PC lamellae the CTTF shifts its pass-band to the right (Fig. 7a). Contrary to the creep of the periodic step response of $G_i(s)$ (Fig. 6a), $N_{pm}(s)$ shows a relaxation of the core (0th layer) for step compression at different (mth) layers. Time constants of $N_{pm}(s)$ for lower $m\,(\leq 15)$ are found to be significantly higher than those of larger $m\,(>15)$, as a lower value of m indicates that the step compression is applied nearer to the core (0th layer). It is also clear from Fig. 7a bottom that for a larger $m\,(>15)$, the PC IC relaxes within 1 ms against a step compression at the PC at mth layer.

Variation of CTTF ($N_{pm}(s)$) in terms of a pole-zero map. Similar to the poles and zeros of $G_i(s)$, Fig. 7b shows the pole-zero map of the CTTF $N_{pm}(s)$ which is a minimal realization with order reduction below 100. In contrast to the pole-zero maps of Fig. 6b, the damping factor of the under-damped poles and zeros of Fig. 7b remains as small as 50 percent, causing relatively higher overshoot in the sub-Hz and MHz ranges. The presence of the over-damped largely-spaced poles and zeros after an angular frequency of $2\pi 100$ rad/s (Fig. 7b 2,2 and 3,1) causes slope variation in the magnitude spectrum of the CTTF especially for larger m ($10 < m \leq n$).

3.4 Simulation of Radial Compression of Layers

In order to describe how the input stimulus at the nth layer gets high-pass filtered at different (ith) internal layers, the compression of different layers is shown in Fig. 8a where layers ($0 \leq i \leq n$) are sampled at every 10 percent of $n = 30$ (periodic trapezoidal stimulus of 25 Hz with 32 μm radial compression and period to rise-time ratio = 16). The simulated compression is measured radially with respect to the central axis of the PC, denoted as radial compression, whereas the compression mentioned in [4] is measured with respect to the diameter across the central axis. In contrast to Fig. 7, Fig. 8 considers the input compressive stimulus only at the outermost (nth) layer, which makes the $i \leq 15$ characteristics relax faster than $i > 15$. Similar to the trapezoidal compression, Fig. 8b shows radial compression of different layers for sinusoidal stimulus (100 Hz and 1 μm) at the outermost layer of the PC ($i = n$). Figs. 8a and 8b indicate that the OC and OL gradually filter the low-frequency components of the input stimulus. Therefore, with the decrease of layer index (i), the negative phase increases in the trapezoidal stimulus and the phase shift of compression also increases in the sinusoidal stimulus. On the other hand, the LL probably acts more as a protective cover for the capsule rather than taking part in high-pass filtering of the stimulus. It also prevents the saturation of the interlamellar space in OC and OL.

To compare the simulated result with the experimental results of approximately 800 μm diameter PC [4], we have chosen $n = 60$ and outer diameter = 864 μm (Table 2; Sample 6 of Fig. 3a). The motion of the layers at the zone boundary (Table 2) is shown in Fig. 8c. Due to the high-pass filtering of the input trapezoidal signal, the compression of the IC and OC appears as a pulse train. The width of the pulse obtained from this simulation with a similar trapezoidal stimulus as in [4] is found to be 6 ms, which is a good match for the experimental data [4]. According to [4], in the OC ($R_i < 25\%$ of R_n) the lamellae motions are dominated by dynamic (high-frequency) components compared to its static (low-frequency) component. This model also shows the similar dominance of a dynamic component for the OC lamellae (Fig. 8c). It is worth noting that although the model [3] approximately matches 6-ms pulse width, it fails to show significant attenuation of low-frequency components at the OC mainly due to its limitations as mentioned in the Section 2.4. Apart from the radial compression of the layer at the zone boundaries, the attenuation of low-frequency components is clearly visible in the form of a percentage inter-layer strain of an individual layer ($(x_i(t) - x_{i-1}(t))/(R_i - R_{i-1}).100\%$) as shown in Fig. 8d.

3.5 PC Size versus Zone Boundary and its Relaxation

The size of a PC can be described in terms of either its number of layers (n), or the outermost radius (R_n). Depending on the size, the zone boundaries of the PC layers show different relaxation patterns. The variation of the PC zone boundary due to the size of the PC and its biomechanical response is summarized in Table 2. Although in this model the $\hat{R}_n$ (approximate radius of the outermost lamella from microscopic slides) and n can be independently selected (7), the relation of R_n versus n becomes unique due to the constraint of maximum interlamellar spacing = 12 μm in (7), as shown in Fig. 3b and Fig. 9a row 1. With the variation of n, not only does the radius of the outermost layer R_n alter nonlinearly but so do the boundaries of the internal zones in terms of $\%R_n$ (Fig. 9a rows 2 and 3). It is worth noting that for all n, the zone boundaries are defined by the fixed set of $\%n$ [0 percent, 10 percent, 40 percent, 90 percent, 100 percent] (Table 2).

As shown in Fig. 9b, the compression relaxation time constants of the IC and GZ vary nonlinearly with the total number of lamellae (n). One common feature of the characteristics of Fig. 9b is that all the relaxation time constants of the IC increase monotonically with the increase of n. However, such monotonicity is not maintained for the GZ lamellae. Against the step compression at the outermost lamellae

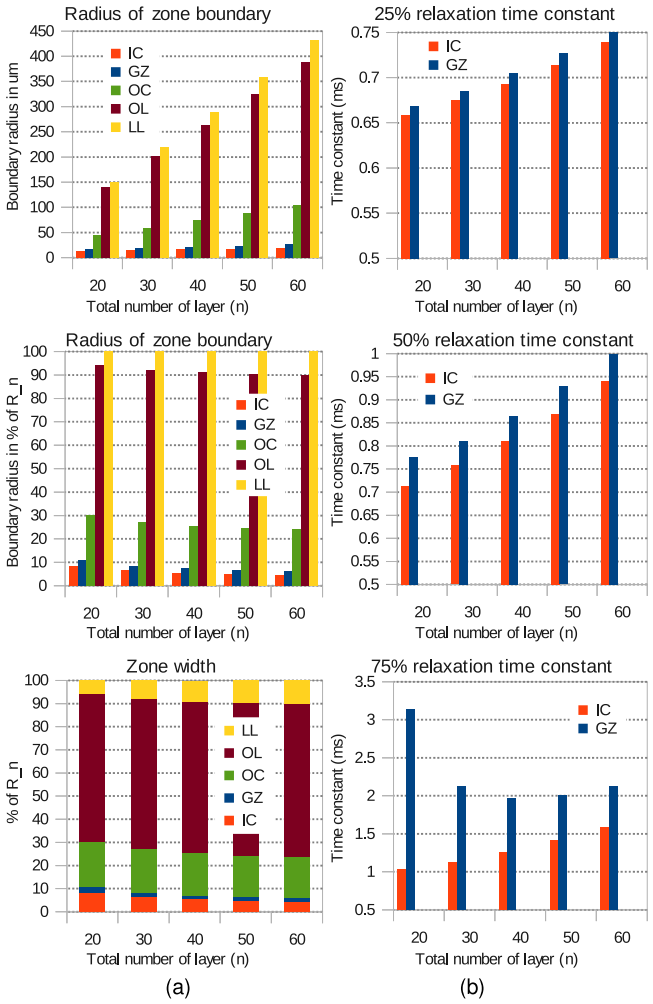

Fig. 9. (a) Variation of zone boundary and zone width depending on the number of layers (*n*). (b) Variation of IC and GZ relaxation time constants due to step compression at the outermost layer of the PC; IC: Inner Core; GZ: Growth Zone; OC: Outer Core; OL: Outer Lamellae; LL: Limiting Lamellae (Fig. 1 and Table 2).

of the PC, the lamellae present after the OC have a very large compression relaxation time constant (Table 2) and hence are not shown in Fig. 9b. It is worth noting that as the step compression is directly applied on the outermost lamella ($m = n$), the zone boundary of the LL cannot relax at all, which is represented by the time constant $= \infty$ in Table 2. For IC, the increase of time constants related to compression relaxation (Fig. 9b) is actually caused by the shift of the pass-band of the $N_{pm}(s)$ with the increase of n. Such a shift of the pass band has a similarity with the reduction of the cut-off of the lamellar high-pass filter as the layer index (m) increases (Fig. 7). The 3 dB cut-off of $N_{pn}(s)$ for a below-40-layer PC is found to be in the range of 1–2 kHz and it goes below 1 kHz if the number of layers is increased further (Samples 5 and 6 in Fig. 3a).

4 Discussion

PC Size and Lamella Distribution. One of the major contributions of this work is the formulation of a better analytical relationship between the radius of the PC outermost layer (R_n) and the number of layers (n). The size and lamella distribution of the PC are empirically estimated from the recently published high-magnification microscopic slides and the description of lamellar structure as in [1], [6], [8], [9], [10] along with the low-magnification slides and the description in [1], [4]. This in turn shows that Hubbard's analytical relationship [1], [4] holds good only for the small PCs or PCs with augmented OL. The proposed model describes more a generalized relationship (7) between the radius of different layers (R_i) and the layer index (i) considering the IC as the 0^{th} layer. Therefore, it can also systematically categorize the different zones of the capsule, with an indication of the range of the radius and the number of layers in different zones. The analytical relationship for a 30-layer PC is quantitatively compared with the data available from [3], [4] and it was found that the proposed relationship is a good fit even for the small PCs ($n = 30$ in Fig. 4 and Table 1). Along with the 30-layer PC, using the same analytical relationship, six different sizes of PCs are simulated ($R_n = 150$ to 432 μm). Although these six PCs (Fig. 3 and Table 2) contain different numbers of layers ($n = 20$, 25, 30, 40, 50 and 60) and radii, they have a common maximum interlamellar spacing of 12 μm (10–15 μm), which appears to be a more generalizable property for the different PCs described in [1], [4], [6], [8], [10], as shown in Fig. 3. This model also captures 3–4 percent reduction in R_n to $\hat{R}_n$ using (7) when the PC layers are punctured [1], [2].

Biomechanical characteristics of the PC lamellar structure. Another contribution of this model is the formulation of recursive transfer functions related to complex compliance $G_i(s)$ and CTTF $N_{pm}(s)$ of different layers of the PC. The frequency response of $G_i(s)$ indicates that the outermost layer of the PC can be a few 1,000 times stiffer in the kHz range compared to the sub-Hz range (6). Similarly, the frequency response and periodic step response of CTTF $N_{pm}(s)$ clearly describes the high-pass filtering effect of the lamellar structure. It is also observed that with the increase of size and layer number, the cut-off frequency of the lamellar high-pass filter drops which makes the pass-band wider and the PC more sensitive toward relatively low-frequency stimulus (Figs. 7 and 9b). Such lowering of the cut-off frequency probably indicates the reason why young people are more sensitive to high-frequency vibration than older people [33], as it is well known that the PC increases in size and number of layers with age [5], [34]. However, one advantage of larger PCs as predicted from this model is that they have higher detectability to a random stimulus as they have a wider pass band. This actually helps in compensating the extra attenuation of stimulus for the subcutaneous PCs as they are typically found to be larger in size than the PCs in dermis [1], [34], [35].

Material properties of the PC. The response of this model is significantly sensitive to the material properties of the PC used for calculating the system parameter K_{pi}, K_{si} and B_{si} of the biomechanical model. For the simulation, a reasonable range of elastic modulus of lamellae (E_L) and viscosity of interlamellar matrix (U) is found to be 1-2 kPa and 1.5-7 mPa. s respectively. Apart from B_{si}, as obtained from the chosen viscosity (5), the viscous frictional coefficient of the IC ($B_{s0} = B_{sc}$ of Fig. 2) is another sensitive parameter, considered as 0.0255 N.s.m^{-1}, which is 5-10 times lower than the minimum of B_{si} for $0 < i \leq n$. It controls the peak percentage

strain at the IC (Fig. 8d). In the chosen PC model, the outermost layer can undergo compression beyond 20 percent of R_n without saturation of the interlamellar space in the capsule or excessive compression of the IC.

Order of the model. In the proposed model, the PC IC is considered as Voigt's model with a serial spring resulting in a first order bi-proper transfer function if the mass is neglected and becomes second order bi-proper if the mass-effect is included. This can also be approximated as the first or second order bi-proper version of Kelvin's model. However, with alteration of the mass position in Kelvin's model as shown in [28] the transfer function becomes strictly-proper third order (8), which has the inherent limitation of creating high-frequency jitters in transits while attempting to simulate low-frequency creep simultaneously.

Effect of mass. From this simulation it is found that the effect of mass is negligible in the functional range of the PC (a few 10s of Hz to a few kHz). However, the effect of mass is clearly observable in terms of under-damped poles and zeros in the frequency range >1 MHz (Figs. 6, and 7 pole-zero map 3,2). If the PC core is modeled as a third order transfer-function similar to (8) the effect of mass is observable even below 1 MHz. In comparison to mass, the response of this proposed model is found to be more sensitive on the viscosity and elastic modulus of the interlamellar matrix as well as that of the lamellae.

Core relaxation and validation. The developed model is validated with the experimental data in [4] considered as a benchmark. When the outermost lamella of the PC is stimulated with a step indentation, the IC relaxes within 1 ms for small- and medium-size PCs ($n < 40$ in Fig. 3a). However, as the PC selected by Hubbard in his experiment is larger in diameter (800 μm) it creates $\sim$6 ms pulse of indentation against trapezoidal stimulus [4], which matches this simulation result (Fig. 8c). However, against the step indentation, even such large PCs show 90 percent relaxation of the IC within 2 ms. As the core follows higher-order relaxation characteristics, Table 2 summarizes them in terms of 25, 50 and 75 percent relaxation time constants for all the six selected PCs (Fig. 3a).

Improvement over existing models. The proposed model is significantly different from several simple biomechanical models which approximate the PC lamellar filter as a linear combination of differentiators of different orders [13], [18], [36] for directly matching the mechanical stimulus to a neural response. The proposed model is not only capable of showing the differentiation process, but also the zone where it occurs (around the OC). The LL and the OL mostly drift instead of differentiating the trapezoidal stimulus, which in turn helps in stabilizing the OC and preventing the saturation of the interlamellar space. Therefore, interlamellar spacing plays a significant role in defining the frequency response of this biomechanical filter. Unlike the existing models, the proposed model uses the material properties of the PC, such as the viscosity of the interlamellar matrix and the viscous frictional coefficient of the IC, which are important in governing the response of the lamellar filter. Although this model assumes homogeneous material properties due to the lack of explicit data available in the literature, it has provision for incorporating inter-layer heterogeneity. The layerwise inhomogeneity can also be assessed by the reverse estimation of the model parameters from the experimental data as in [4].

Computational accuracy in simulation. Apart from a detailed model, this paper describes methods for achieving better computational accuracy in the simulation of biomechanical responses of the PC. One major challenge in this simulation is the consideration of the mass. The pole-zero map of the complex-compliance ($G_i(s)$) and the CTTF ($N_{pm}(s)$) indicates that the poles and zeros contributed by the mass belong to the MHz range (Figs. 6 and 7) and, therefore, they can be safely neglected in the functional range of the PC (a few 10s of Hz to a few kHz). This simplification also reduces the order of the transfer functions $G_i(s)$, $Q_i(s)$ and $N_{pm}(s)$, which helps in simulating the compression signal for the PCs with layer number $n > 30$. If the effect of mass is considered, the order of the $N_{pm}(s)$ crosses 500 even for n = 30 in a non-minimal realization of the transfer functions. Therefore, to restrict the order of the transfer functions below 100 in their minimal realization, the tolerance for pole-zero cancellation is selected in-between $\text{eps}^{0.5}$ and $\text{eps}^{0.1}$, where eps is the machine epsilon (2.2204e-16). This introduces a little inaccuracy in the simulation in frequency only below 0.1 Hz. However, a higher tolerance for pole-zero cancellation can cause significant inaccuracy even below 1 Hz, hence is avoided in this simulation. The requirement of the minimal realization is observable from the pole-zero map of the transfer functions (Figs. 6 and 7). More than the high-frequency under-damped poles and zeros, the sub-Hz under-damped poles and zeros make the model's stability vulnerable, as computational error accumulates during simulation and a few of the poles may gradually shift to the right half of the s-plane. However, the model's stability and computational accuracy is improved by neglecting the mass-effect and reducing the model order with minimal realization of the transfer functions. From Fig. 6 it is clear that the damping factor of the under-damped poles and zeros in complex compliance can be around 90 percent, causing very little overshoot in the sub-Hz and MHz ranges. It is interesting to note that in the functional range of the PC the poles and zeros of $N_{pm}(s)$ remain over-damped, whereas in the sub-Hz range they can be significantly under-damped (damping factor $\approx$ 50 percent). From the frequency response and pole-zero map of $N_{pm}(s)$ (Fig. 7) it is fair to conclude that the lower cut-off of $N_{sp}(s)$ remains in the order of 1 kHz and the bandwidth extends beyond 10 kHz which helps in maintaining VT sensitivity beyond 1 kHz [37], [38], [39].

Limitations of the model. This simulation considers the linear biomechanical model as the stimulus amplitude typically remains below 100 μm in the functional frequency range of the PC, causing less than 20 percent strain in any layer. Therefore, considering [40], [41] it appears that for such a small compression, the PC biomechanics would remain significantly linear. However, for a larger stimulus it is found that the lamellae of two consecutive layers may touch each other, causing a higher degree of nonlinearity, which may be addressed by considering piecewise linear biomechanical properties for different ranges of stimulus. It is worth noting that the direct simulation of the IC compression using the approximated $N_{pm}(s)$ (14) as described in the Section 2.5, introduces <2% error compared to an iterative

layer-wise simulation of the IC compression. Although compared to [3] this model can show higher attenuation of the static component in the OC compression that matches well with the experimental result of [4], the attenuation of the static component of the IL and OL remains lower in the response of the proposed model compared to [4]. One of the major reasons of this mismatch is probably the interlamellar inhomogeneity of the material properties as well as the approximation of the PC as concentric cylinders. While the model has a provision to account for the depth of the PC in the skin, in this paper the interaction between the skin and the PC is not detailed, as it is out of the scope of this paper.

5 Summary

This paper not only describes a layered analytical model of the PC lamellar structure but also generalizes the model over various sizes of the PC. It also summarizes the details of the lamellar structure reported in recent literature and takes them into account in order to improve the accuracy of the model. The simulated response of the model for a 30-layer PC matches well with the experimental result in literature. Therefore, the proposed model can be considered as a major improvement over the existing simple biomechanical models as well as the detailed model from [3]. Although the main objective of this paper is to analyze the effect of size variability of the PC on the relaxation response only, it can also be extended to study this effect on the well known U-shaped neural response of the PC [30], [31]. In spite of its few limitations, this model has potential in simulating a network of various PCs for investigating the mechanism of enhancing the high-frequency vibration perception through the skin. The model can also be adopted for simulating and analyzing the physiology of other corpuscular lamellar mechanoreceptors like Herbst's corpuscle [42], [43], typically found in non-mammalian species such as birds.

Acknowledgments

A. Biswas is the corresponding author.

References

[1] J. Bell, S. Bolanowski, and M. H. Holmes, "The structure and function of Pacinian corpuscles: A review," *Progress Neurobiol.*, vol. 42, no. 1, pp. 79–128, Jan. 1994.

[2] D. C. Pease and T. A. Quilliam, "Electron microscopy of the Pacinian corpuscle," *J. Biophys. Biochem. Cytol.*, vol. 3, no. 3, pp. 331–342, 1957.

[3] W. R. Loewenstein and R. Skalak, "Mechanical transmission in a Pacinian corpuscle. An analysis and a theory," *J. Physiol.*, vol. 182, no. 2, pp. 346–378, Jan. 1966.

[4] S. J. Hubbard, "A study of rapid mechanical events in a mechanoreceptor," *J. Physiol.*, vol. 141, no. 2, pp. 198–218, 1958.

[5] N. Cauna and G. Mannan, "The structure of human digital Pacinian corpuscles (corpus cula lamellosa) and its functional significance," *J. Anatomy*, vol. 92, no. 1, pp. 1–20, 1958.

[6] P. Dubovy and J. Bednarova, "The extracellular matrix of rat Pacinian corpuscles: An analysis of its fine structure," *J. Anatomy Embryol.*, vol. 200, pp. 615–623, May 1999.

[7] B. Munger, Y. Yoshida, S. Hayashi, T. Osawa, and C. Ide, "A re-evaluation of the cytology of cat Pacinian corpuscles," *Cell Tissue Res.*, vol. 253, no. 1, pp. 83–93, 1988.

[8] L. Pawson, N. B. Slepecky, and S. J. Bolanowski, "Immunocytochemical identification of proteins within the Pacinian corpuscle," *Somatosensory Motors Res.*, vol. 17, no. 2, pp. 159–170, 2000.

[9] L. Pawson and S. J. Bolanowski, "Voltage-gated sodium channels are present on both the neural and capsular structures of Pacinian corpuscles," *Somatosensory Motors Res.*, vol. 19, no. 3, pp. 231–237, 2002.

[10] K. Sames, Z. Halata, M. Jojovic, E. J. M. van Damme, W. J. Peumans, B. Delpech, B. Asmus, and U. Schumacher, "Lectin and proteoglycan histochemistry of feline Pacinian corpuscles," *J. Histochem. Cytochem.*, vol. 49, no. 1, pp. 19–28, Jan. 2001.

[11] H. Irie, T. Kato, T. Yakushiji, J. Hirose, and H. Mizuta, "Painful heterotopic pacinian corpuscle in the hand: A report of three cases," *Hand Surg.*, vol. 16, no. 01, pp. 81–85, 2011.

[12] F. Vaes and L. D. Smet, "A rare cause of digital pain: The subepineural Pacinian corpuscle," *Eur. J. Plastic Surg.*, vol. 26, no. 7, pp. 370–372, 2003.

[13] F. Grandori and A. Pedotti, "Theoretical analysis of mechano-to-neural transduction in pacinian corpuscle," *IEEE Trans. Biomed. Eng.*, vol. BME-27, no. 10, pp. 559–565, Oct. 1980.

[14] M. H. Holmes and J. Bell, "A model of a sensory mechanoreceptor derived from homogenization," *SIAM J. Appl. Math.*, vol. 50, no. 1, pp. 147–166, 1990.

[15] L. J. Drew, F. Rugiero, and J. N. Wood, "Touch," in *Mechanosensitive Ion Channels, Part B*, vol. 59, O. P. Hamill, Ed. New York, NY, USA: Academic Press, 2007, pp. 425–465.

[16] L. Malinovský, L. Pác, J. A. Vega-Alvarez, and W. Bozilow, "The capsule structure of Pacinian corpuscles from the cat mesentery," *Zeitschrift Mikroskopisch Anatomische Forschung*, vol. 104, no. 2, pp. 193–201, 1990.

[17] B. L. Munger and C. Ide, "The enigma of sensitivity in Pacinian corpuscles: A critical review and hypothesis of mechano-electric transduction," *Neurosci. Res.*, vol. 5, no. 1, pp. 1–15, Oct. 1987.

[18] S. Bensmaia, S. S. Kim, A. Sripati, and R. J. Vogelstein, "Conveying tactile feedback using a model of mechanotransduction," in *Proc. Biomed. Circuits Syst.*, 2008, pp. 137–140.

[19] J. Bell and M. H. Holmes, "A note on modeling mechano-chemical transduction with an application to a skin receptor," *J. Math. Biol.*, vol. 32, no. 3, pp. 275–285, 1994.

[20] L. Yang, "*Mechanical properties of collagen fibrils and elastic fibers explored by AFM*," Ph.D. dissertation, Polymer Chemistry and Biomaterials, Biomedical Sciences, Faculty of Science and Technology, Univ. of Twente, Enschede, Netherlands, 2008.

[21] F. H. Silver, G. P. Seehra, J. W. Freeman, and D. DeVore, "Viscoelastic properties of young and old human dermis: A proposed molecular mechanism for elastic energy storage in collagen and elastin," *J. Appl. Polym. Sci.*, vol. 86, no. 8, pp. 1978–1985, Jan. 2002.

[22] K. Gelse, E. Poschl, and T. Aigner, "Collagens-structure, function, and biosynthesis," *J. Adv. Drug Del. Rev.*, vol. 55, pp. 1531–1546, Aug. 2003.

[23] M. P. Jacob, "Extracellular matrix remodeling and matrix metalloproteinases in the vascular wall during aging and in pathological conditions," *J. Biomed. Pharmacotherapy*, vol. 57, no. 5/6, pp. 195–202, 2003.

[24] G. A. Holzapfel, *Collagen: Structure and Mechanics*. Heidelberg, Germany: Springer, 2008.

[25] W. Xu, R. Mezencev, B. Kim, L. Wang, J. McDonald, and T. Sulchek, "Cell stiffness is a biomarker of the metastatic potential of ovarian cancer cells," *PLoS ONE*, vol. e46609, 2012, doi:10.1371/journal.pone.0046609

[26] E. A. G. Peeters, D. L. Bader, F. P. T. Baaijens, C. W. J. Oomens, and C. V. C. Bouten, "Viscoelastic properties of single attached cells under compression," *J. Biomech. Eng.*, vol. 127, no. 2, pp. 237–243, Sep. 2004.

[27] S. Newman, M. Cloître, C. Allain, G. Forgacs, and D. Beysens, "Viscosity and elasticity during collagen assembly in vitro: Relevance to matrix-driven translocation," *Biopolymers*, vol. 41, no. 3, pp. 337–347, 1997.

[28] A. Biswas, M. Manivannan, and M. A. Srinivasan, "A biomechanical model of Pacinian corpuscle & skin," in *Proc. Biomed. Sci. Eng. Conf.*, 2013, pp. 1–4.

[29] B. Rydqvist, N. Purali, and J. Lannergren, "Visco-elastic properties of the rapidly adapting stretch receptor muscle of the crayfish," *Acta. Physiol. Scand.*, vol. 150, no. 2, pp. 151–159, 1994.

[30] A. Biswas, M. Manivannan, and M. Srinivasan, "Nonlinear two stage mechanotransduction model and neural response of pacinian corpuscle," in *Proc. Biomed. Sci. Eng. Conf.*, 2014, pp. 1–4.

[31] A. Biswas, M. Manivannan, and M. A. Srinivasan, "Vibrotactile sensitivity threshold: Nonlinear stochastic mechanotransduction model of the Pacinian corpuscle," *IEEE Trans. Haptics*, DOI: 10.1109/TOH.2014.2369422.

[32] X. Yang and C. C. Church, "A simple viscoelastic model for soft tissues the frequency range 6–20 MHz," *IEEE Trans. Ultrason., Ferroelectr., Freq. Control*, vol. 53, no. 8, pp. 1404–1411, Aug. 2006.
[33] C. Wells, L. M. Ward, R. Chua, and J. T. Inglis, "Regional variation and changes with ageing in vibrotactile sensitivity in the human footsole," *J. Gerontol. A Biol., Sci. Med. Sci.*, vol. 58, no. 8, pp. 680–686, Aug. 2003.
[34] K. Kumamoto, H. Senuma, S. Ebara, and T. Matsuura, "Distribution of Pacinian corpuscles in the hand of the monkey, Macaca fuscata," *J. Anatomy*, vol. 183, pp. 149–154, 1993.
[35] Z. Halata, "The ultrastructure of the sensory nerve endings in the articular capsule of the knee joint of the domestic cat (Ruffini corpuscles and Pacinian corpuscles)," *J. Anatomy*, vol. 124, no. 3, pp. 717–729, 1977.
[36] R. G. Dong, S. Rakheja, T. W. McDowell, D. E. Welcome, and J. Z. Wu, "Estimation of the biodynamic responses distributed at fingers and palm based on the total response of the hand–arm system," *Int. J. Ind. Ergonom.*, vol. 40, no. 4, pp. 425–436, 2010.
[37] L. D. Goodfellow, "Vibratory sensitivity: its present status," *Psychol. Bull.*, vol. 31, no. 8, pp. 560–571, Oct. 1934.
[38] V. O. Knudsen, "'Hearing' with the Sense of Touch," *J. Gen. Psychol.*, vol. 1, no. 2, pp. 320–352, 1928.
[39] L. Wyse, S. Nanayakkara, P. Seekings, S. H. Ong, and E. Taylor, "Perception of vibrotactile stimuli above 1 kHz by the hearing-impaired," presented at the 12th Int. Conf. New Interfaces Musical Expression, Ann Arbor, Michigan, USA, University of Michigan, 2012.
[40] L. Barbé, B. Bayle, M. de Mathelin, and A. Gangi, "Needle insertions modeling: Identifiability and limitations," *Biomed. Signal Process. Control*, vol. 2, no. 3, pp. 191–198, 2007.
[41] R. J. Gulati and M. A. Srinivasan, "Determination of mechanical properties of human fingerpad in vivo using a tactile stimulator," M.S. Thesis, Touch Lab MIT Report 3, RLE TR-605, College of Engineering, Boston University and Touch Lab MIT, Massachusetts, USA, 1997.
[42] K. M. Gottschaldt, H. Fruhstorfer, W. Schmidt, and I. Kräft, "Thermosensitivity and its possible fine-structural basis in mechanoreceptors in the beak skin of geese," *J. Comparative Neurol.*, vol. 205, no. 3, pp. 219–245, 1982.
[43] P. H. J. Nafstad and A. E. Andersen, "Ultrastructural investigation on the innervation of the Herbst corpuscle," *Z. Zellforschung Und Mikroskopische Anatomie*, vol. 103, no. 1, pp. 109–114, 1970.

Abhijit Biswas received the BTech degree in electronics and instrumentation from the University of Kalyani and the ME degree in biomedical engineering from Jadavpur University, Kolkata, in 2006 and 2008, respectively. He worked at Robhatah Robotic Solutions Pvt. Ltd., a spin-off company of the National University of Singapore, as a senior R&D engineer for two years and joined Touch Lab, IIT Madras, as a research scholar.

M. Manivannan received the ME and PhD degrees from the Indian Institute of Science, Bangalore. He received post-doctoral training in Haptics at MIT, Cambridge. Before MIT, he received another post-doctoral training in CAD standards and sensors network at the National Institute of Standards and Technology, Maryland. He served as a chief software architect of Yantric Inc. before joining IIT Madras.

Mandayam A. Srinivasan received the PhD degree from the Department of Mechanical Engineering at Yale University. He is the founder and director of the MIT Touch Lab, and a senior research scientist at MIT's Department of Mechanical Engineering and the Research Laboratory of Electronics. He is also Professor of Haptics in the Department of Computer Science, University College London, United Kingdom. His research interests include haptic computation, cognition, and communication in humans and machines, particularly to enhance human–machine interactions in virtual reality and teleoperation systems.